Scientific and technical results from VINCI using coherent estimation of fringe visibility *

J. A. Meisner
Leiden Observatory

Abstract. Although primarily intended as a test and alignment instrument in order to commission the VLTI, VINCI has taken useful scientific data in its first year and a half of operation. Our results employ coherent integration of fringe visibility in which the actual amplitudes of the raw scans are combined linearly after correcting for the position of the fringe within each scan. In addition to reducing the effect of noise compared to incoherent integration, the result contains a broader range of information, including an estimate of the complex visibility spectrum.

Such an estimator is thus sensitive to instrumental phase and spectral characteristics, including the variable component of dispersion introduced by the excess air paths in the delay lines. Calibration of such instrumental effects demonstrates the ability to detect source phase at a fine level as will be required for direct interferometric detection of extrasolar planets.

We present diameters for five stars obtained by observing the visibility null in their correlated spectra. Using coherent integration we have also observed the peculiar correlated spectra seen in many Mira variables, possibly due to changes in the apparent diameter with wavelength. Calibration of the zero-baseline power from o Ceti is used with other interferometric observations of this star over a period of 90 days to plot diameter variations associated with its pulsation cycle.

Keywords: Stellar interferometry, coherent integration, phase, VINCI, VLTI

1. Introduction

VINCI[3] is the first interferometric instrument installed on the VLTI and has been in operation since March 2001. Primarily intended as a test and alignment instrument in order to commission the VLTI, its design was based on the FLUOR instrument[1]. Like FLUOR, VINCI operates at 2 microns (K band) using single spatial mode interference employing optical fibers for spatial filtering and beam combination. The interferometric signal is temporally modulated using delay-scanning.

In a year and a half of service, VINCI has made over 7000 interferometric observations (raw visibilities), from which significant astronomical results have been derived. We report here on results employing *coherent* methods of fringe visibility estimation, Among other advantages, such techniques are capable of obtaining the (optical) spectrum

* VINCI data included herein is based on observations made with the European Southern Observatory telescopes obtained from the ESO/ST-ECF Science Archive Facility.

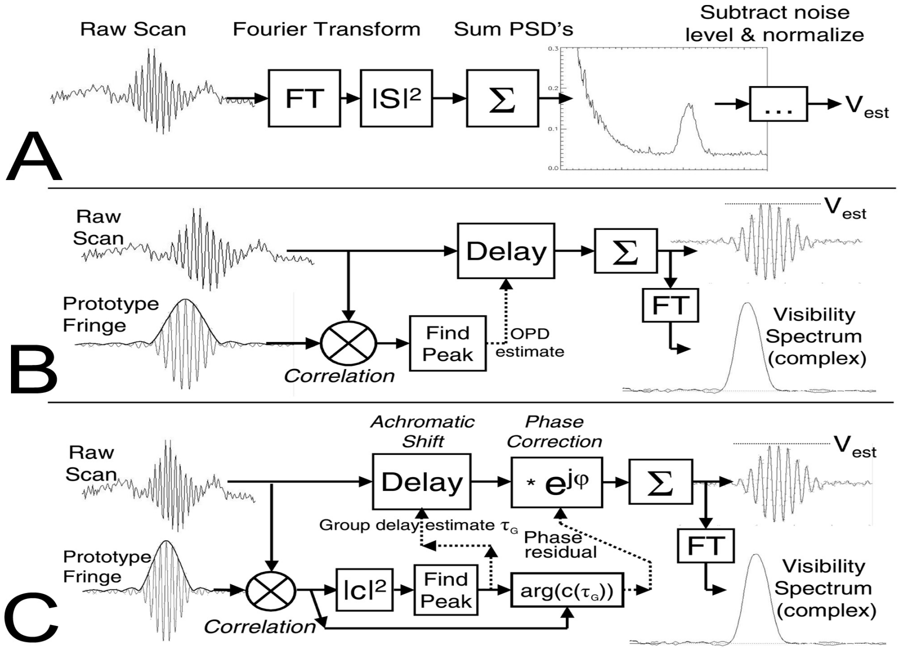

Figure 1. **A.** *Incoherent* integration of fringe visibility sums the spectrum of each individual scan. The net power spectrum contains a noise pedestal, above which the integrated amplitude due to interference yields the squared magnitude of visibility. **B.** *Coherent* integration centers each scan by correlating it with a "prototype fringe." The fringe amplitudes are then summed, to yield an actual estimate of the underlying fringe (right) from which a complex spectrum can be obtained. **C.** *Quasi-coherent* integration is similar, but each scan is centered using the *group delay* (envelope) estimator. An additional phase correction is then required to force cophasing, as the error of the group delay estimator is generally greater than a radian. The first order term of dispersion (spectral phase variation around center frequency) is destroyed by this processing which forces the phase delay at the center frequency to match the group delay prior to integration.

of correlated flux including the *phase* of interference over that spectrum. However the opportunity to garner such information requires increased levels of instrumental calibration and characterization. In this paper we shall briefly describe the data reduction methods involved, the instrumental calibration procedures applied, and a few preliminary scientific results obtained using such methods.

2. Data Reduction Methods

The success of FLUOR, from which the design of VINCI was derived, was in large part due to its innovative use of single mode optical fibers. The consequent spatial filtering of the input beams enabled a high precision and repeatability of interferometric visibilities, at the 1% level, without being highly sensitivity to changes in atmospheric seeing. Differential dispersion due to unequal fiber lengths was tolerated by employing long scans which sampled the thereby broadened fringe packet, and a visibility estimator[2] which is utterly insensitive to dispersion. This is done by accumulating the power spectra but discarding the phase of interference on a scan-by-scan basis (Fig. 1A).

Results in this paper, however, employ *coherent* integration methods, in which the actual *amplitudes* of the fringe packets are co-added (Fig. 1B). This produces a linear estimate of the visibility spectrum without introducing the noise pedestal. With a semi-narrowband instrument such as VINCI, there is an advantage in the *quasi-coherent* method (Fig. 1C), which does not presuppose unambiguous identification of the central fringe in each scan. This entails loss of the linear term of the visibility phase, which is difficult to estimate anyway with a narrowband instrument (except with a very high SNR). Random atmospheric dispersion fluctuations[4] which are largely first order in phase, are conveniently ignored by the estimator. All results presented in this paper employ quasi-coherent integration of fringe visibility; one may compare a (complex) correlated spectrum so obtained with the square root of the incoherently integrated power spectrum plotted in Fig. 3A (dotted line).

3. Calibration of Visibility Phase

Although the "zero-delay" reference point of an interferometric observation is arbitrary, one can observe the *relative* phase delays of spectral components in the visibility curve. The phase we then measure includes both the true source phase plus instrumental components. Thus retrieval of the source phase is dependent on calibration of the instrumental phase function.

The instrumental phase has a fixed component due to the fiber beam combiner (and other optical elements in the beams' paths) plus a component due to unequal path lengths through dispersive air in the delay lines and light paths. Therefore if we can determine the fixed instrumental phase function of the optical components and beam combiner $\Phi_B(\nu)$, and we know the phase function per meter of delay line air $d\Phi_A/dl$, then knowing the excess air path D for a particular observation, we can find the true source phase $\Phi_{CORR}(\nu)$ from the raw visibility phase Φ_{RAW} as follows.

$$\Phi_{CORR}(\nu) = \Phi_{RAW}(\nu) - \Phi_B(\nu) - \frac{d\Phi_A(\nu)}{dl} \cdot D \tag{1}$$

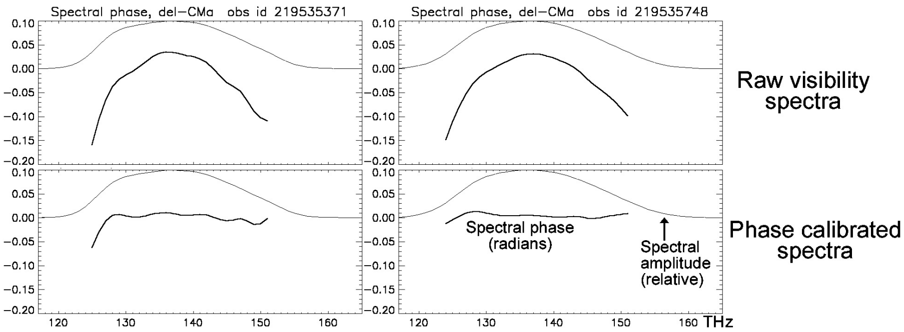

Figure 2. **Top:** Raw visibility phase as a function of optical frequency for two high SNR observations of δ CMa. Phase in radians plotted in bold versus optical frequency. Thin plot is the relative spectral amplitude of correlated flux, depicting energy in the K band from 125 THz (2.4 μm) to 150 THz (2.0 μm).
Bottom: Residual phase functions following calibration of beam combiner phase and excess air path dispersion as described in the text.

The coefficient of the delay line component of dispersion, $d\Phi_A/dl$, may be based on a physical model[4], and can be verified by comparison of observations using different air paths D during a single night during which the beam combiner phase function $\Phi_B(\nu)$ was stable. More careful monitoring of the humidity in the VLTI tunnels, along with barometric and temperature measurements already recorded, will be required to fully compensate for the variable component of dispersion. Given that calibration of the dispersive air, the fixed instrumental component of spectral phase $\Phi_B(\nu)$ can be obtained from one or more calibrator observations, using stars expected to have symmetric structure (and thus zero phase). That instrumental phase function has been observed to change radically when adjustments to the fiber beam combiner have been performed, but appears to usually remain stable during a given night.

In Fig. 2 the visibility phase over the K band is shown for two observations of δ CMa on 13 October 2001. Since these reductions used the quasi-coherent technique, first order components of the phase function are absent. The remaining phase function is largely instrumental in origin, and is greatly reduced after phase correction using (1), as seen in the bottom graphs of Fig. 2. The residual phase has thereby been reduced to about .01 radians rms which is at the level of the measurement noise of these observations. Programs underway to interferometrically detect the light of extrasolar planets will require such phase calibration an order of magnitude better still.

4. Stellar Diameters from Visibility Nulls in the Spectra

One interesting feature found in several VINCI observations, occurs when the effective baseline samples the spatial frequency $f_{null} = 1.22/D$, at which the visibility of a star with a uniform disk diameter D crosses zero. This will occur, for a geometric baseline B, at the optical frequency $\nu_{null} = c f_{null}/B$. If that optical frequency lies within the instrument's passband, then the visibility will cross zero at that point. Such a determination of a stellar diameter is not dependent on the instrument's visibility calibration (transfer function).

Fig. 3A shows the spectrum of α Sco (obtained through quasi-coherent integration) observed on 2 April 2001. Ignoring the non-zero imaginary part of the spectrum (surely due to an asymmetric feature in the source), we can see that the visibility crosses zero at an optical frequency of 143.3 THz (2.09 μm). At the baseline length of 14.96 meters, this implies a spatial frequency of $f_{null} = 34.7\, arcsec^{-1}$ corresponding to a diameter (uniform disk model) of $1.22/f_{null} = 35.2\, mas$.

In Fig. 3B we have used an observation of α Ori performed just past the first visibility null. An approximate "calibration" of the spectrum has been performed by dividing the coherently integrated spectrum obtained by that of an arbitrary calibration star. The resulting (negative) visibility has a shape which is reasonably well matched to the expected curve shown in a dashed line; the extrapolated position at which the observed visibility crosses zero again supplies an estimate of the uniform disk diameter. Further results obtained in this manner from several VINCI observations are detailed in the following table.

Object Name	Observation JD-2450000	Baseline (meters)	P.A.	Null Frequency (THz)	(arcsec^{-1})	UD Diam (mas)
α Sco	2001.41747	14.96	9.5°	143.3	34.67	35.19
	2001.42195	14.81	8.8°	144.7	34.65	35.20
	1991.37136	15.99	20.4°	129.2	33.41	36.52
α Her	1998.40935	15.91	16.2°	150.8	38.80	31.44
	1998.41386	15.95	16.6°	149.8	38.64	31.57
	2001.35130	14.73	12.9°	162.0*	38.59	31.61
α Ori	2195.34149	14.66	15.6°	117.5*	27.86	43.80
W Hya	2297.27323	12.53	59.0°	120.5*	24.42	49.97
o Ceti	2295.05506	14.34	17.7°	149.3	34.62	35.24
	2295.05907	14.17	17.9°	150.1	34.39	35.47

* Frequency of a *projected* null, outside of the instrument's passband.

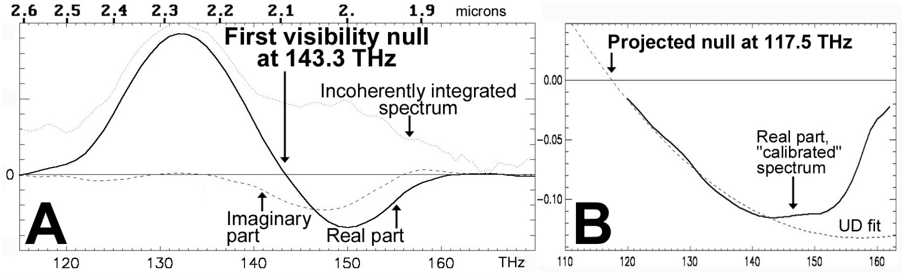

Figure 3. **A.** Zero-crossing of real part of coherently integrated visibility spectrum of α Sco allows for diameter determination. **B.** Visibility curve of α Ori "calibrated" using instrumental spectrum of an average star. Fit to theoretical UD visibility function shown, with projected null just outside of instrumental passband.

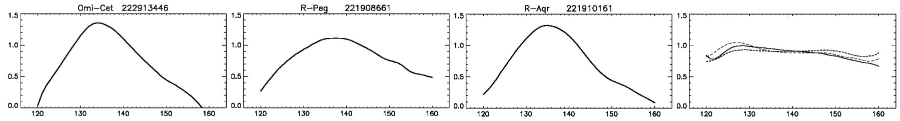

Figure 4. Spectra of correlated flux relative to "calibration" star for 3 Mira variables. **Right:** Calibrated spectra of 3 random stars for comparison.

The diameters found here for o Ceti are also plotted as triangles in Fig. 5C. The 11% larger diameter found using this method, compared to the fit based on broadband visibilities, could possibly be attributed to a wavelength-dependence in the effective diameter. The larger diameter listed in the above table reflects the UD diameter at 150 THz (2.0 μm) whereas the broadband visibility is dominated by power centered around 135 THz (2.2 μm).

5. Visibility Spectra of Mira's and Diameter Determinations

One remarkable effect noticed in the spectrally resolved visibility curves is found in the case of Mira variables. Most of the Mira's observed with VINCI produce spectra which, when compared to typical stars (to account for the instrumental spectral response) are peaked around 135 THz (2.2 μm), but which fall off at both lower and higher frequencies. Three examples are shown in Fig. 4, in which the relative visibility spectra of o Ceti, R Peg, and R Aqr are shown after dividing by the visibility spectrum of ψ Phe. Similarly obtained spectra of three random stars are plotted in the rightmost panel for comparison purposes.

It is suspected that the reduction in correlation toward the edges of the K band is evidence of an effective diameter increase at these wavelengths due to an extended stellar atmosphere, as has previously been observed interferometrically[5] in such stars. Such an overresolved

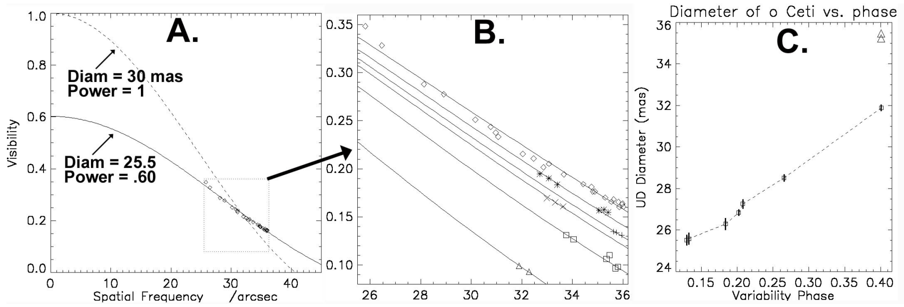

Figure 5. **A.** Visibility vs. baseline using a "normal" UD model is rejected in favor of a model with a zero-baseline power reduced to .60. **B.** Detail of the nightly fits for each of the diameter solutions modelled using this zero-baseline power. **C.** Solutions of the (UD) diameter variations over 90 days of this star's variability cycle.

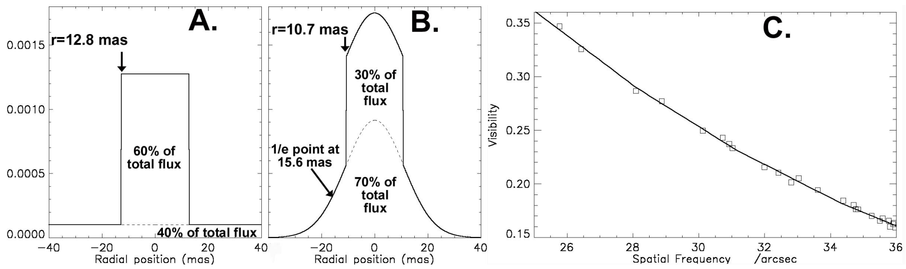

Figure 6. **A.** Two-parameter solution, with 60% of flux in a uniform disk of diameter 25.55 mas. Region containing the remaining flux is considered to be highly overresolved (level shown for illustrative purposes only). **B.** Three-parameter solution as described in text. **C.** Fit of visibility predicted by three-parameter solution to data.

region would have little contribution to the broadband visibility, leaving only the contribution from a more compact photosphere responsible for the correlated flux at intermediate wavelengths.

Further evidence of the existence of infrared emission in an extended region is provided by fitting of visibilities observed on 7 nights between October 2001 and January 2002 using a 16 meter physical baseline. 25 visibility points observed on 23 and 24 October 2001 are plotted in Fig. 5A. A "normal" 30 mas diameter uniform disk fit to these visibilities shown with the dashed line clearly fails. A reasonably good fit, however, is obtained with the visibility curve for a 25.5 mas uniform disk *when reduced* by the factor 0.60. This would be consistent, for instance, with a model in which 60% of the light emanated from a compact photosphere with this diameter, and the remaining light was uncorrelated (therefore having zero contribution to the net visibility), perhaps because it emanated from a very extended region which was overresolved at these baselines (see Fig. 6A).

We attempted to fit the data from each of the 7 nights using this two-parameter model as detailed in the following table. During four of these nights there was sufficient projected baseline coverage to solve for the proportion of "correlatable power," that is, the position on the visibility curve that would be extrapolated at zero spatial frequency (as depicted in Fig. 5A). The resulting proportion, 0.60, was then forced to apply to the model for each of the seven nights, to deduce the variation in diameter over time as plotted in Fig. 5C. Note that this assumption, that the zero-baseline power proportion was constant, is not well founded. However independent estimations on the four nights in which this was possible are consistent with a constant value. Fig. 5B shows the fits of visibility versus projected baseline on each night using the final diameter solutions listed in the following table.

Datapoints			**Zero-baseline power**		**Diameter (mas)**	
JD	Phase	Num	Estimated	rms	Estimated	rms
Independent nightly solutions used to estimate zero-baseline power						
2205	.13	13	.622	.019	25.80	.28
2206	.13	12	.609	.016	25.68	.22
2223	.18	6	.568	.021	25.84	.22
2250	.27	6	.599	.048	28.48	.44
Average			.6024	.010		
Solutions assuming estimated zero-baseline power determined above						
2205	.13	13	(.6024)	.010	25.52	.23
2206	.13	12	(.6024)	.010	25.58	.26
2223	.18	6	(.6024)	.010	26.30	.26
2229	.20	3	(.6024)	.010	26.84	.13
2231	.21	3	(.6024)	.010	27.26	.20
2250	.27	6	(.6024)	.010	28.52	.15
2295	.40	2	(.6024)	.010	31.88	.13

The visibility determinations employed the quasi-coherent estimator, from which only the real parts of the visibility at each optical frequency were summed to compute the net visibility. Thus additional noise from the imaginary parts of these visibilities was rejected; imaginary components of the visibility are not consistent with a symmetric source structure as required by this model. In fact, it was found that the rms of the imaginary part of these visibilities was usually less than .005, thereby placing a tight upper limit on the magnitude of source asymmetries which are resolvable using these baselines.

Although the two-parameter fit to the 25 visibilities obtained on 23 and 24 October 2001 (Fig. 5B, top curve) is not bad, systematics in the residual errors can be observed which are inconsistent with uncorrelated noise. Applying a three-parameter fit to these data, it was possible to reduce the rms amplitude of the residual error by a factor of two, thus justifying such an approach. The stellar image is assumed to be radially symmetric, including a wide gaussian circumstellar envelope whose $1/e$ radius is to be solved for. Added to that is the flux from a compact photosphere, modeled as a uniform disk with a diameter which is also solved for. The third model parameter, again, is the proportion of flux received from each component. The net solution is depicted in Fig. 6B with the solution parameters labelled.

It must be emphasized that this solution is certainly not unique among three-parameter models, and the specific model invoked is unrealistic if considered in detail. However the remarkable reduction in the χ^2 of the fit thus obtained, by adding only one degree of freedom, is sufficient to conclude that the underlying image at these wavelengths is better described by the solution shown in Fig. 6B rather than the simpler two-parameter model (Fig. 6A). The fit to the visibility data shown in Fig. 6C may be compared to the poorer fit using the simple two-parameter model as seen in the top curve of Fig. 5B. Such a "parametric imaging" capability represents the best that can be hoped for using high precision data points (SNR > 100) obtained over a very limited range of baselines before the first visibility null.

References

1. Coude Du Foresto, V., G. Perrin, C. Ruilier, B. P. Mennesson, W. A. Traub, and M. G. Lacasse: 1998, 'FLUOR fibered instrument at the IOTA interferometer'. In: *Proc. SPIE Vol. 3350, p. 856-863, Astronomical Interferometry, Robert D. Reasenberg; Ed.*, Vol. 3350. pp. 856–863.
2. Coude Du Foresto, V., S. Ridgway, and J.-M. Mariotti: 1997, 'Deriving object visibilities from interferograms obtained with a fiber stellar interferometer'. *Astronomy and Astrophysics Supplement series* **121**, 379–392.
3. Kervella, P., V. Coude du Foresto, A. Glindemann, and R. Hofmann: 2000, 'VINCI: the VLT Interferometer commissioning instrument'. In: *Proc. SPIE Vol. 4006, p. 31-42, Interferometry in Optical Astronomy, Pierre J. Lena; Andreas Quirrenbach; Eds.*, Vol. 4006. pp. 31–42.
4. Meisner, J. and R. Le Poole: 2002, 'Dispersion affecting the VLTI and 10 micron interferometry using MIDI'. In: *Proc. SPIE Vol. 4838, Interferometry for Optical Astronomy II*, Vol. 4838.
5. Mennesson, B., G. Perrin, G. Chagnon, V. C. d. Foresto, S. Ridgway, A. Merand, P. Salome, P. Borde, W. Cotton, S. Morel, P. Kervella, W. Traub, and M. Lacasse: 2002, 'Evidence for Very Extended Gaseous Layers around O-rich Mira Variables and M Giants'. *Astrophysical Journal* **579**, 446–454.